Received: 22 July 2021 | Revised: 12 May 2022 | Accepted: 15 June 2022

DOI: 10.1049/rpg2.12535

IET Renewable Power Generation

The Institution of Engineering and Technology WILEY

ORIGINAL RESEARCH

Maximum power point tracking-based model predictive control with reduced sensor count for PV applications

Mostafa Ahmed[1,2] | Ibrahim Harbi[1,3] | Christoph M. Hackl[4] | Ralph Kennel[1] | Jose Rodriguez[5] | Mohamed Abdelrahem[1,2]

[1]Chair of High-Power Converter Systems, Technical University of Munich (TUM), Munich, Germany

[2]Electrical Engineering Department, Faculty of Engineering, Assiut University, Assiut, Egypt

[3]Electrical Engineering Department, Faculty of Engineering, Menoufia University, Shebin El-Koum, Egypt

[4]Department of Electrical Engineering and Information Technology, Munich University of Applied Sciences, Munich, Germany

[5]Faculty of Engineering, Universidad San Sebastian, Santiago, Chile

Correspondence
Mostafa Ahmed, Chair of High-Power Converter Systems, Technical University of Munich (TUM), 80333 Munich, Germany.
Email: mostafa.ahmed@tum.de

Abstract

This paper discusses the MPPT based on finite-set model predictive control (FS-MPC) in photovoltaic (PV) systems. Generally, the FS-MPC implementation needs more sensors in comparison with the traditional methods due to the existence of the prediction stage. However, it has a fast transient behaviour in case of fast-changing atmospheric conditions. Thus, to make benefit from the FS-MPC principle without increasing the system's cost, two algorithms are developed to reduce the number of required sensors without altering the efficiency. First, an accurate model of the PV system including the losses is derived, which enables estimation of the output capacitor voltage. Another approach utilizing an extended Kalman filter (EKF) is proposed. The EKF takes advantage of the derived model of the system and estimates the PV current. In addition, practical PV system applications are considered to have an estimate for cost reduction with the proposed methods. The proposed methodologies are compared with the conventional FS-MPC with full sensor utilization, where analysis and evaluation of the current- and voltage-oriented FS-MPC methods are presented. Moreover, robustness assessment of the proposed algorithms with sensor reduction against parameter variation is examined. All studied methods are validated in simulation and experimentally at different operating conditions.

1 | INTRODUCTION

1.1 | Photovoltaic (PV) energy and need for maximum power point tracking (MPPT)

PV energy is considered one of the fastest growing sources of renewable energy ones. The abundance, cleanliness, silent operation, low maintenance, and almost free emissions – all these special properties – force different countries to adopt PV energy as a substitutional source for the conventional fossil energy sources [1–3]. The depletion nature of fossil resources necessitates the existence of alternative sources. Furthermore, environmental issues related to the traditional sources make the transition to renewable energy sources inevitable. Moreover, recently different countries are enforcing numerous regulations to reduce CO_2 emissions, which makes renewable energy installation an obligation rather than an option [3–5]. However, low-energy conversion efficiency and the non-linear behaviour of the PV source entail MPPT to maximize energy harvesting from the PV system [5].

To implement the maximum power point algorithm, an additional component (power converter) is added between the PV source and the load. Different topologies of converters are installed in the PV systems with the intent of interfacing the load with the PV source. However, the most widespread one is the boost converter, especially when considering grid connection [6]. Briefly, the PV source is followed by a boost converter to enable the MPPT implementation. Thus, to increase the PV system's efficiency, the PV cell technology, the converter design (topology), and the MPPT technique are the crucial elements to be examined in this arrangement [7]. In this regard, the MPPT algorithm is the most cost-effective approach to be considered [7]. Accordingly, many MPPT techniques were developed and presented in the literature [8–10]. These methods are different with respect to their implementation, cost, efficiency, number of required sensors, transient behaviour (tracking speed), and so forth [8]. Nevertheless, the most popular techniques for MPPT are the perturb and observe (P&O), hill climbing, incremental conductance (INC) [11], constant voltage, fractional open-circuit voltage, and fractional short-circuit current technique [12]. However, these methods suffer either from slow transient responses and oscillations around the maximum power point (MPP) or inaccurate power capturing [13]. Furthermore, potential losses happen due to PV power interruptions during open-circuit voltage or short-circuit current measurements [14, 15].

Recent methods also utilize fuzzy logic controllers, and artificial neural networks [12]. However, they need a lot of tuning and training efforts [15, 16]. Even more, soft computing methods are also addressed [17], which include particle swarm optimization (PSO), simulated annealing, genetic algorithm, wolf gray optimization, bat technique, ant colony, and so forth [18]. These methods are intended for the extraction of maximum power at partial shading conditions, where the power–voltage (P–V) characteristic shows several maxima. In general, these approaches suffer from a high computational burden due to their searching nature. Furthermore, the partial shading methods require complex algorithms and implementation, which in turn needs a fast controller. This of course increases the cost of the system. Therefore, the PV companies are not ready for such techniques. Thus, improvement of the conventional and low-cost methods is the preferred solution from a practical and industrial point of view [19].

1.2 | Previous work on MPPT-based model predictive control (MPC)

Recently, MPC is employed for different control purposes in different power converters and drives [20]. It can be classified into three essential categories: Predictive dead-beat control, continuous-set MPC, and finite-set model predictive control (FS-MPC) [21]. The FS-MPC is the most familiar approach due to its intuitive and simple principle. Furthermore, no modulators are needed in this scheme. The discrete-time model of the system allows predicting the best or optimal switching state of the converter according to quality function design [6]. Many efforts have been made to exploit the FS-MPC technique for maximum power extraction in PV systems [7, 13, 22–29]. Table 1 summarizes these endeavours.

As a summary of the table, one can observe that the FS-MPC technique requires more sensors in comparison with the classical techniques. For example, P&O or INC methods use two sensors (one voltage sensor and one current sensor) to generate the reference for the linear controller (proportional-integral (PI) controller). Even for direct control, where the control parameter is the duty cycle itself, also two sensors are used. However, for the FS-MPC, two sensors are used for reference generation. The reference can be current or voltage based on the outer loop, which is normally the P&O or INC. Additional sensors are required within the prediction stage, in which the optimal switching state is applied directly to the power switch. Clearly, the selection of this state is based on the evaluation of the cost function. That number of sensors is related to the states of the power converter. This, in turn, increases the system's cost, especially when considering low-power PV applications, where the cost of the system itself is compared to the cost of the utilized sensors. Furthermore, this reduces the reliability of the PV system.

1.3 | Sensor reduction for MPPT-based MPC

Limited number of studies attempts to reduce the number of required sensors for MPPT in PV systems. In [7], a methodology based on the MPC principle is suggested for the flyback converter. However, the ideal model of the converter is utilized in this method. Similarly, a simple model for a multi-level boost in [24], and an ideal model of high gain DC–DC converter in [30] are used to decrease the sensor count, where the approach utilized there is based on mathematical modelling of the utilized converter. Sensor reduction is preferred to decrease the cost and achieve high control performance in case of sensor failure. This encourages the authors to develop two strategies for sensor reduction.

Considering the above, two reduced sensor count algorithms are presented in this study. The first approach uses the model of the PV system to estimate the control parameter. To be specific, the studied system consists of a PV generator, boost converter, and resistive load. The model of the boost converter is developed including the dominant losses of the converter. Thus, the capacitor voltage (output voltage) can be estimated according to this model. A second approach employs an extended Kalman filter (EKF) to eliminate the current sensor. Both algorithms are integrated into the FS-MPC for implementation. Furthermore, the P&O method is utilized for reference generation. Other advanced methods can also be integrated with the proposed methodology for reference generation. However, to sustain the simplicity of the controller, the P&O or the INC is preferred for implementation (see Table 1). The proposed techniques are evaluated at different operating conditions using simulation and experimental results. In addition, the robustness of the studied methods is investigated. The main contributions of this paper can be summarized as follows:

- Providing a review of the voltage- and current-oriented techniques for MPPT-based FS-MPC. Furthermore, comparison and evaluation of these methods.
- Detailed modelling of the PV system including losses analysis to simplify sensorless control of the PV system.

TABLE 1 Previous work on MPC for MPPT

Cited reference	Year of publication	Converter topology	Number of sensors	Implementation	Remarks
[7]	2017	Flyback converter	2	Experimental	INC is utilized with FS-MPC. The current sensor is removed based on the MPC approach. Furthermore, a simple load observer is incorporated.
[13]	2014	Flyback converter	3	Simulation	FS-MPC is integrated with INC method to enhance its transient behaviour.
[22]	2011	Boost converter	3	Simulation	INC method is combined with two-step prediction FS-MPC.
[23]	2013	Boost converter	4	Experimental	P&O method with certain modifications to enhance the performance is implemented with various voltage-based and current-based FS-MPC techniques.
[24]	2017	Multilevel boost converter	2	Experimental	INC method is used with the FS-MPC technique. Sensor reduction is achieved using a simplified model for the multi-level converter.
[25]	2016	Boost converter	2	Experimental	Fixed switching frequency method, which is based on prediction model using Thévenin equivalent circuit of the PV source. However, the duty cycle command is obtained utilizing a PI controller.
[26]	2016	Z-source inverter	2	Experimental	Similar of the above-mentioned approach, that is [25].
[27]	2019	Buck converter	3	Experimental	Technique for fast-changing atmospheric conditions is implemented, which combines the FS-MPC and the model of the PV source for performance enhancement.
[28]	2019	Boost converter	3	Experimental	Revised version of the P&O method with single-step prediction is implemented for the FS-MPC approach.
[29]	2020	Boost converter	2	Simulation	P&O technique is used to generate the reference for the FS-MPC. The required sensors are reduced by utilizing an extended Kalman filter (previous work of the authors).

- Elimination of the voltage sensor at the output of the boost converter using an accurate losses model of the PV system.
- Current sensorless approach utilizing EKF. Furthermore, robustness assessment of the proposed techniques.
- Considering sensor reduction, a detailed analysis of cost reduction for different practical PV systems is investigated to show the effectiveness of the proposed strategies.

In summary, only two sensors are used for maximum power harnessing as in the case of the traditional methods. However, the controller implementation is based on the FS-MPC for transient behaviour enhancement. Thus, the proposed methodology suits well low-power PV applications.

The rest of this paper is arranged as follows: Section 2 provides the detailed model of the PV system. The conventional MPPT methods are reported in Section 3, and the proposed reduced sensor count techniques are investigated in Section 4. Simulation studies, cost calculation, and experimental results of all methods are discussed in Section 5. Finally, the outcome of the study is given in Section 6.

2 | MODELLING OF THE PV SYSTEM

According to the single-exponential model of the PV system, the P–V and I–V curves of the PV source (KC200GT) at various radiation conditions are shown in Figure 1.

The boost converter has two modes of operations, which are specified by the actions of its power switch, that is, OFF and ON states. Most of the studies in the area of MPPT use simple representation for the converter model by neglecting the losses [7, 13, 22, 23, 28, 29]. However, in the present study, an accurate model is developed to imitate the real situation as closely as possible. This model is very important when considering sensor reduction, which is the current objective of our study. As neglecting the losses will lead to inaccurate estimation. Furthermore, the errors in the estimation may lead to losing the goal of MPPT by capturing other operating points. Considering that, the inductor resistance, the voltage drops across the power switch, and the diode are incorporated in the utilized model. Figure 2 shows the topology of the boost converter with the two modes of operation, where the PV module is acting as a feeding source. Based on that, the response of the boost converter at OFF operation can be described as

$$\frac{di_l}{dt} = -\frac{r_l}{L} i_l + \frac{1}{L}(v_{pv} - v_d - v_c), \tag{1}$$

$$\frac{dv_c}{dt} = \frac{1}{c}\left(i_l - \frac{v_c}{R}\right), \tag{2}$$

where i_l is the inductor current, v_c is the output capacitor voltage, L is the boost inductance, r_l is the inductor parasitic resistance, v_d is the drop across the diode at conduction state, c is the output capacitor value, and R is the resistive load.

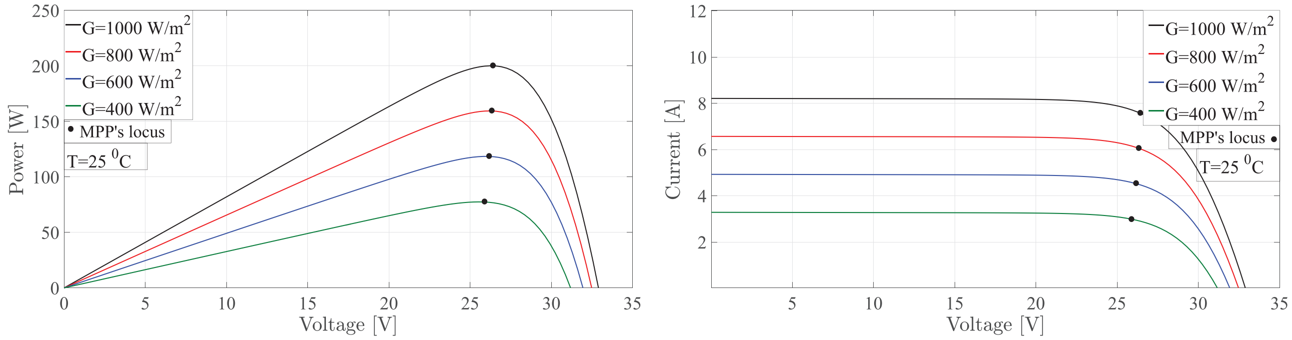

FIGURE 1 P–V and I–V characteristics of the PV source at different radiation conditions

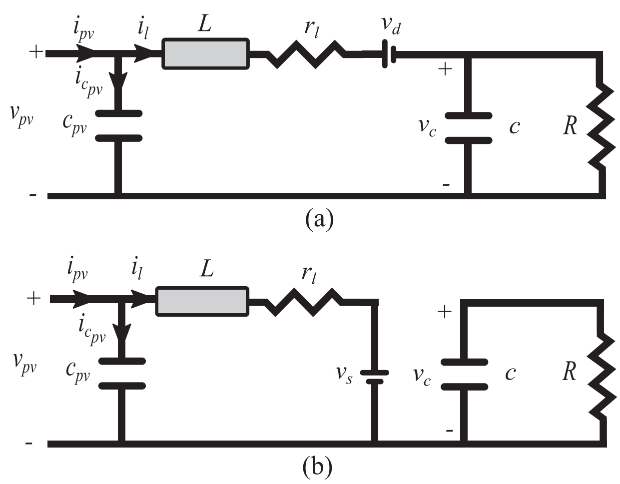

FIGURE 2 Operation modes of the boost converter: (a) Switch is OFF; (b) Switch is ON

Furthermore, when the switch is ON:

$$\frac{di_l}{dt} = -\frac{r_l}{L}i_l + \frac{1}{L}(v_{pv} - v_s), \tag{3}$$

$$\frac{dv_c}{dt} = -\frac{1}{Rc}v_c, \tag{4}$$

where v_s is the drop across the switch at ON state. The final model of the boost converter can be summarized as

$$\begin{aligned} \dot{x} &= \mathbf{A}x + \mathbf{B}u, \\ y &= \mathbf{C}x + \mathbf{D}u, \end{aligned} \tag{5}$$

where $x = [i_l \;\; v_c]^{\mathrm{T}}$ is the state vector, $u = (v_{pv} - v_s)$ is the input, $y = v_c$ is the output, and assuming v_s=v_d. Hence, **A**, **B**, **C**, and **D** are the model matrices, and they are expressed as follows:

$$\mathbf{A} = \begin{bmatrix} -\frac{r_l}{L} & -\frac{1-d}{L} \\ \frac{1-d}{c} & -\frac{1}{Rc} \end{bmatrix}, \; \mathbf{B} = \begin{bmatrix} \frac{1}{L} \\ 0 \end{bmatrix},$$
$$\mathbf{C} = \begin{bmatrix} 0 & 1 \end{bmatrix}, \; \mathbf{D} = 0, \tag{6}$$

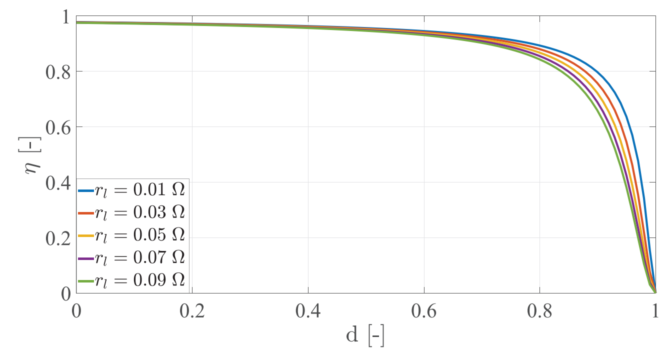

FIGURE 3 Efficiency variation of the boost converter with the duty cycle at various values of the inductor resistance

where d is the duty cycle. At steady state, the efficiency of the boost converter can be evaluated by

$$\eta = \frac{(1-d)^2 i_o R}{(1-d)^2 i_o R + (1-d)v_s + i_o r_l}, \tag{7}$$

where i_o is the average value of the output current of the boost converter (load current). Figure 3 shows the efficiency of the boost converter as a function of the duty cycle. Notably, the efficiency drops at high duty cycle values. Therefore, it is vital to account for that decrease in designing the operating region of the converter. Moreover, as the parasitic resistance of the inductor increases, the efficiency further decreases.

3 | CONVENTIONAL MPPT METHODS USING FS-MPC

MPPT-based FS-MPC is implemented commonly using two approaches, which are voltage-based MPPT and current-based one. For both, any method can generate the reference (voltage or current) for the FS-MPC technique. However, the most popular methods for reference generation are the P&O method and INC technique. Figure 4 presents the system under research and the basic idea of MPPT with FS-MPC. To implement the FS-MPC, the discrete-time model of the system should be derived. Therefore, the discrete-time equations can be obtained with reference to Equations (1)–(4) as follows:

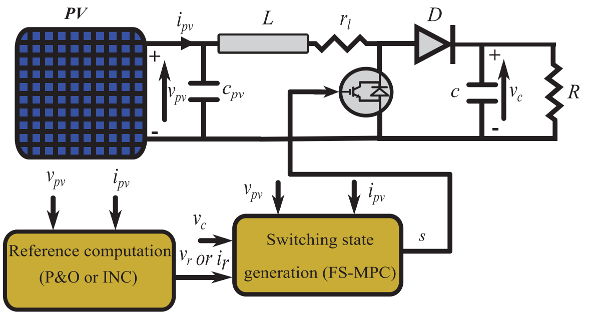

FIGURE 4 Configuration of the PV system with MPPT-based FS-MPC

$$i_{pv}[k+1] = \left(1 - \frac{r_l T_s}{L}\right) i_{pv}[k] + \frac{T_s}{L}(v_{pv}[k] - v_d - v_c[k]), \quad (8)$$

$$v_c[k+1] = \left(1 - \frac{T_s}{Rc}\right) v_c[k] + \frac{T_s}{c} i_{pv}[k], \quad (9)$$

$$i_{pv}[k+1] = \left(1 - \frac{r_l T_s}{L}\right) i_{pv}[k] + \frac{T_s}{L}(v_{pv}[k] - v_s), \quad (10)$$

$$v_c[k+1] = (1 - \frac{T_s}{Rc}) v_c[k], \quad (11)$$

where Equations (8) and (9) represent the OFF state, while Equations (10) and (11) represent the ON state. Furthermore, T_s is the sampling period, $[k+1]$ refers to the predicted sampling instant, and $[k]$ is the present one. It is worth mentioning that $i_{pv} \approx i_l$ when assuming the ripple behaviour of the currents is similar.

3.1 | Current-oriented MPPT

Knowing the predicted PV currents at the two states of the boost converter. Then, the cost function for designing the current-oriented MPPT, as the name implies, is based on the current as follows:

$$g_i|_{s=0,1} = |i_{pv_{s=0,1}}[k+1] - i_r|, \quad (12)$$

where i_r is the reference current coming from the outer loop reference generator.

3.2 | Voltage-oriented MPPT

To implement the voltage-based procedure, the predicted PV voltages should be evaluated. Thus, the voltages are obtained as

$$v_{pv}[k+1] = (1-d) v_c[k+1]. \quad (13)$$

Then, the cost function for best switching state selection is tuned as

$$g_v|_{s=0,1} = |v_{pv_{s=0,1}}[k+1] - v_r|, \quad (14)$$

where v_r is the reference voltage. It is also possible to design the quality function to include both current and voltage as [22, 31]

$$g_{i,v}|_{s=0,1} = \lambda_1 |v_{pv_{s=0,1}}[k+1] - v_r| + \lambda_2 |i_{pv_{s=0,1}}[k+1] - i_r|, \quad (15)$$

where λ_1 and λ_2 are weighting factors to be calibrated. With reference to Equations (8)–(11), executing the prediction stage of the FS-MPC requires another sensor for the output capacitor voltage (v_c). Furthermore, if the PV current (i_{pv}) is different than the inductor current (i_l), an additional sensor will be required. The reference generation loop needs two sensors for the PV voltage and current. Therefore, in total, four sensors are desired. This implies higher costs in comparison with the classical P&O or INC, and is considered a major drawback for the MPPT-based FS-MPC, especially for low-power PV systems, which install a small number of modules in the range of watts.

4 | THE PROPOSED FS-MPC WITH REDUCED SENSOR COUNT

4.1 | Losses model-based sensor reduction

In this method, the output capacitor voltage (v_c) sensor is eliminated. Since the input power is known by sensing the input PV voltage and current, the capacitor voltage can be estimated if an accurate losses model is available. The procedure for estimating the capacitor voltage is summarized as follows:

- The input power is calculated as

$$p_{pv} = p_i = v_{pv} i_{pv}. \quad (16)$$

- The operating range for the duty cycle is specified. The range used in this study is (0.1–0.8) for which the efficiency of the converter is higher than 90%. This range is assigned according to the analytical solution (see Figure 3) and the components of the experimental set-up. However, the upper limit of the duty cycle can be decreased further if the parasitic resistance of the inductor is relatively high.
- The output power is computed as

$$p_o = \frac{v_c^2}{R}. \quad (17)$$

- The efficiency of the boost converter is obtained from

$$\eta = \frac{p_o}{p_i} = \frac{v_c^2/R}{v_{pv} i_{pv}}. \quad (18)$$

- Finally, the output capacitor voltage is estimated as

$$\hat{v}_c = \sqrt{\eta v_{pv} i_{pv} R}. \quad (19)$$

The value of the converter efficiency (η) varies with the duty cycle. Thus, it is proposed in this work to operate at the average value within the specified range of the duty cycle. This will be further investigated in the results section.

4.2 | EKF-based sensor reduction

In this part of the study, the PV current (i_{pv}) sensor is removed by employing an EKF, which is the non-linear version of the Kalman filter [6]. Its implementation also depends on the discrete-time model of the system [6, 21]. Therefore, it can be integrated very well with the idea of FS-MPC. So, the model of the system including disturbance can be written as

$$\begin{aligned} \dot{x} &= \mathbf{A}x + \mathbf{B}u + w, \\ y &= \mathbf{C}x + \mathbf{D}u + v, \end{aligned} \tag{20}$$

where $x = [i_{pv} \quad v_c \quad v_{pv}]^{\mathrm{T}}$ is the state vector, $u = [(v_{pv} - v_s)\ v_c]^{\mathrm{T}}$ is the input vector, $y = [v_{pv}\ v_c]^{\mathrm{T}}$ is the measurement vector, w is the system uncertainties with covariance matrix $\mathbf{Q}$, and v is the measurement noise with covariance matrix $\mathbf{R}$. Furthermore, $\mathbf{A}$, $\mathbf{B}$, $\mathbf{C}$, and $\mathbf{D}$ are the system matrices, and they are given by

$$\mathbf{A} = \begin{bmatrix} -\frac{r_l}{L} & -\frac{1-s}{L} & 0 \\ \frac{1-s}{c} & 0 & 0 \\ 0 & 0 & 0 \end{bmatrix}, \ \mathbf{B} = \begin{bmatrix} \frac{1}{L} & 0 \\ 0 & -\frac{1}{Rc} \\ 0 & 0 \end{bmatrix}, \tag{21}$$

$$\mathbf{C} = \begin{bmatrix} 0 & 0 & 1 \\ 0 & 1 & 0 \end{bmatrix}, \ \mathbf{D} = 0.$$

Therefore, the discrete-time model can be expressed as

$$\begin{aligned} x[k+1] &= \mathbf{A}_d x[k] + \mathbf{B}_d u[k] + w[k], \\ y[k] &= \mathbf{C}_d x[k] + \mathbf{D}_d u[k] + v[k], \end{aligned} \tag{22}$$

where $\mathbf{A}_d = \mathbf{I} + \mathbf{A}T_s$, $\mathbf{B}_d = \mathbf{B}T_s$, $\mathbf{C}_d = \mathbf{C}$, $\mathbf{D}_d = \mathbf{D}$, and $\mathbf{I}$ is the identity matrix. Normally, the system uncertainty and measurement noise are not known, so the EKF is implemented as follows:

$$\begin{aligned} \hat{x}[k+1] &= \mathbf{A}_d \hat{x}[k] + \mathbf{B}_d u(k) + \mathbf{K}[k](y[k] - \hat{y}[k]), \\ \hat{y}[k] &= \mathbf{C}_d \hat{x}[k] + \mathbf{D}_d u[k], \end{aligned} \tag{23}$$

where $\mathbf{K}[k]$ is the Kalman gain, and $\hat{x}[k]$ and $\hat{y}[k]$ are the estimated quantities.

Finally, the design of the EKF can be performed through two stages of prediction and modification. The prediction phase involves the state vector prediction and the covariance matrix error prediction as follows:

$$\hat{x}^{-}[k] = \mathbf{A}_d \hat{x}[k-1] + \mathbf{B}_d u[k-1], \tag{24}$$

$$\mathbf{P}^{-}[k] = f[k]\mathbf{P}[k-1]f[k]^{\mathrm{T}} + \mathbf{Q}, \tag{25}$$

where

$$f[k] = \frac{\partial}{\partial x}(\mathbf{A}_d x[k] + \mathbf{B}_d u[k])|_{\hat{x}^{-}[k]}. \tag{26}$$

The modification or correction stage is developed as

$$\mathbf{K}[k] = \mathbf{P}^{-}[k]\mathbf{C}_d^{\mathrm{T}}\left(\mathbf{C}_d \mathbf{P}^{-}[k]\mathbf{C}_d^{\mathrm{T}} + \mathbf{R}\right)^{-1}, \tag{27}$$

$$\hat{x}[k] = \hat{x}^{-}[k] + \mathbf{K}[k](y[k] - \mathbf{C}_d \hat{x}^{-}[k]), \tag{28}$$

$$\mathbf{P}[k] = \mathbf{P}^{-}[k] - \mathbf{K}[k]\mathbf{C}_d \mathbf{P}^{-}[k]. \tag{29}$$

A key step during the design of the EKF is the choice of the matrices P, Q, and R, which affect the behaviour and convergence of the EKF. Thus, the PSO procedure [3] is used to get an initial guess of these matrices. The tuning process is utilized offline to reduce the computation burden. Further guidelines on the effect of these parameters on the EKF response can be found in [21].

To sum up, two methods are considered here for sensor reduction with the FS-MPC. First, the capacitor voltage is eliminated and estimated using an accurate losses model for the PV system. Thus, in this approach, only two sensors are required (v_{pv} and i_{pv}). The second technique also takes advantage of the developed losses model. However, it employs an EKF to estimate the PV current. Therefore, in this method, voltage sensors across the input and output (v_{pv} and v_c) are used for maximum power extraction. The algorithm of the proposed methods with a reduced number of sensors is shown in Figure 5, where the P&O technique is utilized to generate the reference voltage for the FS-MPC algorithm. Then, the FS-MPC selects the optimal state according to the chosen cost.

5 | EXPERIMENTAL AND SIMULATION STUDIES

5.1 | Performance indices for the MPPT

The performance of the MPPT can be evaluated using the instantaneous efficiency expression as [32, 33]

$$\eta_{pv} = \frac{P_{mppt}(t)}{P_r(t)} \times 100, \tag{30}$$

where P_{mppt} is the maximum power obtained from the PV source under certain MPPT algorithm. It is simply the product of the PV voltage (v_{pv}) and current (i_{pv}), and P_r is the reference power from the data-sheet or calculated analytically according to the PV model (based on the data-sheet information). Furthermore, the average efficiency is determined by

$$\eta_{pv,avg} = \frac{\int P_{mppt}(t)dt}{\int P_r(t)dt} \times 100, \tag{31}$$

where the integration is extended over the operating period of the utilized MPPT algorithm.

The results are divided into two cases of simulation and experimental verification, which will be investigated in the following sections.

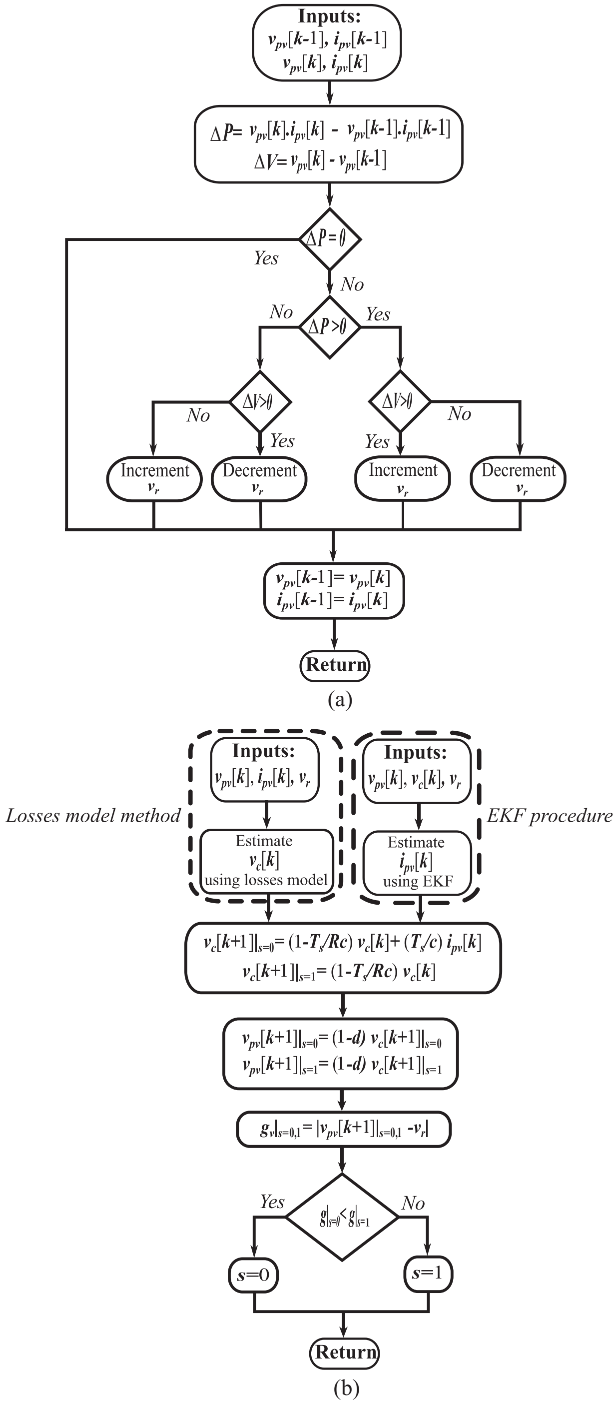

FIGURE 5 The proposed reduced sensor count techniques for MPPT using the losses-based method and EKF: (a) Reference voltage generation using P&O method; (b) FS-MPC procedure for switching state application

5.2 | Simulation and cost calculation

5.2.1 | Simulation case

The performance of the MPPT techniques is studied under different radiation conditions. Two cases of step response and dynamic waveform of the radiation are considered. The ramp profile is chosen to represent the dynamic change of the radiation as recommended by the European standard test (EN 50530) for efficiency evaluation [34, 35].

Figure 6 shows the behaviour of the studied MPPT techniques, which are the current-oriented method with full sensor utilization, the voltage-oriented algorithm (also with full sensors), the reduced sensor count technique based on the losses model, and the EKF approach (reduced sensor). The results in Figure 6 reveal the PV power and the instantaneous efficiency, where all methods succeeded to track the PV power at the sudden change of the radiation. The ripple content of the PV power is approximately 3 W and is very similar for all studied methods despite sensor reduction for some schemes. The instantaneous efficiency of all methods is always kept over 95%.

Furthermore, Figure 7 shows the operation of the PV system under dynamic variation of the radiation. The PV power and the instantaneous efficiency are given in Figure 7 for all considered MPPT approaches. The MPPT techniques can also successfully follow the ramp variation of the radiation. However, the ripple content of the PV power under such a situation is worse than the static condition. The reason is the drift or divergence problem of the MPPT technique [2, 33]. This phenomenon can be simply clarified with the help of Figure 8, where the MPPT is confused under dynamic change of radiation. The MPPT is drifting away from the MPP and following the path indicated in the figure (points 1–6) due to the fast change of the radiation. But the operation under static and normal operation is as indicated by the points 1–3. Nevertheless, still, the efficiency of the MPPT techniques is very satisfactory. However, and compared to the static condition, it is a little bit affected.

Table 2 shows the calculated average efficiency of the MPPT algorithms under the ramp profile of radiation. The MPPT based on current-oriented method has a little bit higher efficiency in comparison with other methods. The voltage-oriented technique, the reduced sensor algorithm-based losses model, and the EKF approach have approximately the same efficiency value.

5.2.2 | Cost reduction computation

In this subsection, the cost of the installation of the PV system is investigated when considering sensor reduction. PV energy is preferred in different applications (stand-alone or grid-connected). Therefore, two systems are considered for this purpose (cost calculation). The first one is the stand-alone street lighting system, which is commonly utilized in isolated areas and also to avoid environmental issues of the conventional sources [36]. Furthermore, the rated power of this system is small, where one PV module can feed the system. Therefore, we have chosen this topology as it is very similar to the experimental set-up of our system (same power level).

The second application (grid-connected), which is an extension of the utilized topology, is the multi-string inverter [37, 38]. Figure 9 shows the configuration of this system, where groups of series-connected modules (called strings) are attached to a DC–DC converter. Then, these converters are connected to an

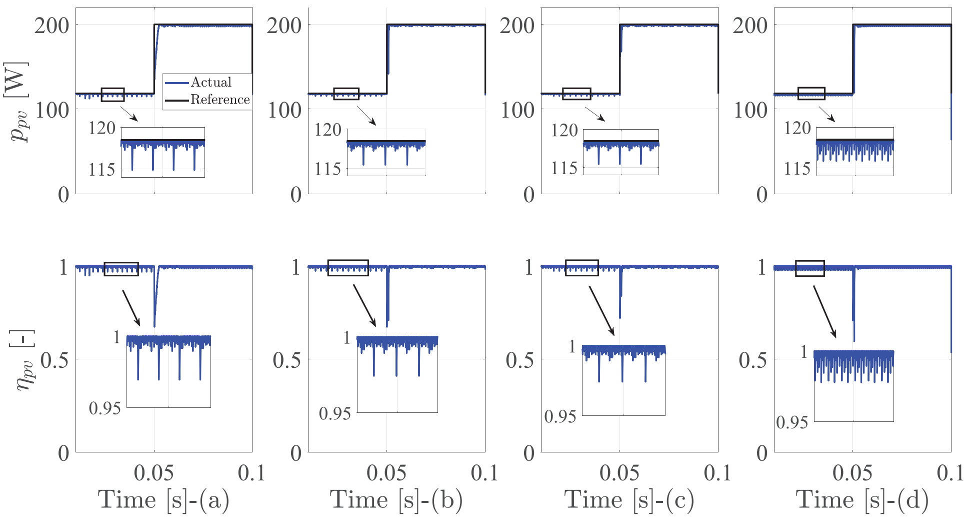

FIGURE 6 Simulation results of the MPPT methods under step change of the radiation: (a) Current-oriented method; (b) Voltage-oriented technique; (c) Reduced sensor count approach based losses model; (d) Reduced sensor count approach based EKF

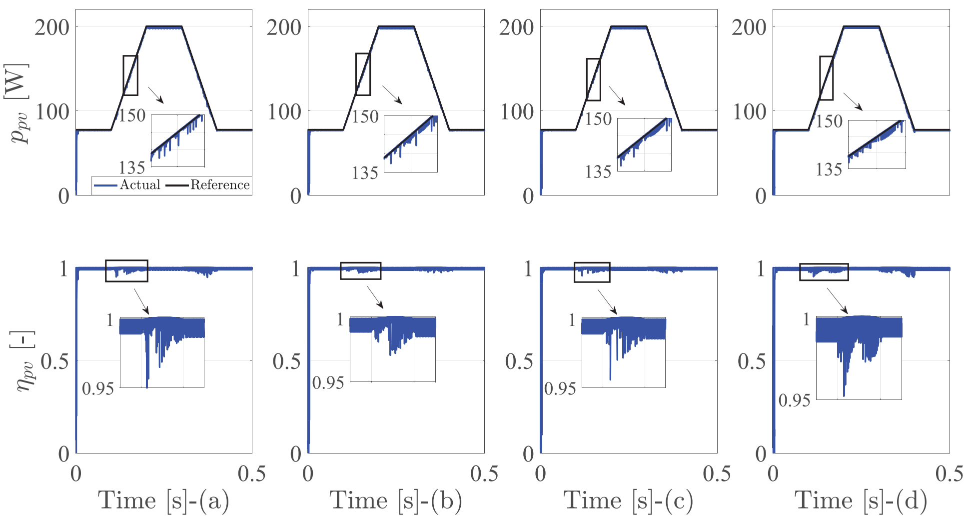

FIGURE 7 Simulation results of the MPPT methods under dynamic radiation profile: (a) Current-oriented method; (b) Voltage-oriented technique; (c) Reduced sensor count approach-based losses model; (d) Reduced sensor count approach-based EKF

inverter through a common DC bus. This topology is preferable due to the simple and separate control and can be extended in structure because of its modularity [38].

Table 3 presents the cost of the main components in the considered PV system. Based on that, the previously mentioned systems (street lighting system and multi-string inverter) are designed and their cost is given in Table 4. The cost is calculated for a unit of the system and a practical system configuration. To be specific, the street lighting system is computed for a 5-km length of road (system1). Furthermore, the assumed power level of the multi-string inverter is 10 kW (system2).

The main components of a single unit of the system are the PV source, boost converter, interfacing circuits, and measurement boards as clarified in the table. The cost of every single component is also given in the table for better documentation and understanding. The prices of the components are obtained from the mentioned websites in the same table. However, it may be subject to change based on the available quantity in the market. The main costs of the system are related to the interfacing circuitry and measurements (sensors), which prove that cost reduction has a strong relation with sensor reduction. In addition, reliability enhancement is an added merit of sensor reduction approaches, where the system operation can be sustained even with sensor failure.

From Table 3, it is quite obvious that the most dominant cost goes for the PV module, the measurement circuits, the inductor, and the gate drive. The PV module is the power source in the system and the gate drive is required for interfacing the control signals with the power circuit. Therefore, the possible reduction of the cost can be achieved based on sensor elimination. However, this should not affect the system behaviour, which inspires the authors to develop two reduced sensor schemes without

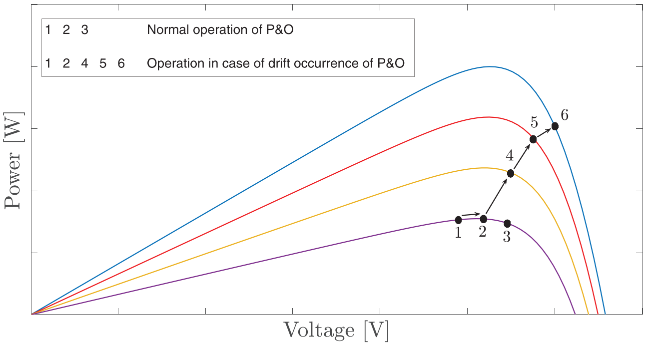

FIGURE 8 The drift phenomenon of MPPT in case of fast radiation conditions

TABLE 2 Average efficiency of the MPPT techniques under dynamic radiation condition

Method	$\eta_{pv,avg}$ (%)
Current-oriented	99.59
Voltage-oriented	99.17
Estimation-based losses model	99.18
Estimation-based EKF	99.21

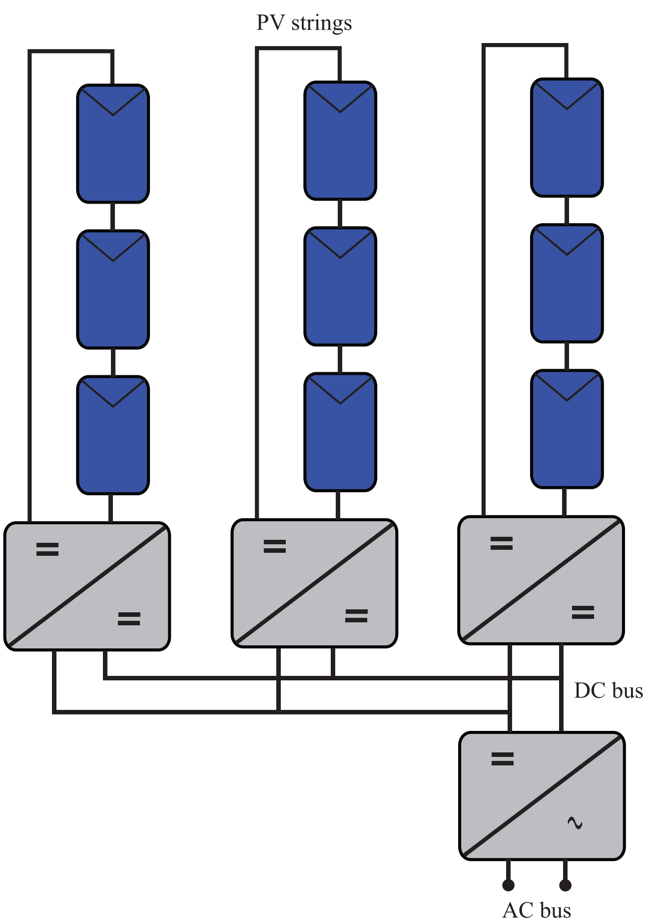

FIGURE 9 Configuration of the multi-string grid-connected PV inverter

TABLE 3 The cost of the main components of the PV system

Unit	Price ($)
Inductor	51.01
Output capacitor	2.37
IGBT	1.69
Diode	2.13
PV module	88.43
Current measurement	66.67
Voltage measurement	66.67
Gate drive	41

Note: Prices of the components are obtained from https://eu.mouser.com & https://www.taraztechnologies.com; Unit price may change based on availability and growth of the market.

TABLE 4 Cost of the PV system installation for practical implementation

Method	System1 ($) A/B	System2 ($) A/B
Current-oriented	386.64/77,328	386.64/19,332
Voltage-oriented	386.64/77,328	386.64/19,332
Estimation-based losses model	319.97/63,994	319.97/15,999
Estimation-based EKF	319.97/63,994	319.97/15,999

Note: A refers to the cost of one unit of the system, and B is the whole cost (5 km road for street lighting & 10 kW for multi-string inverter).

affecting the PV system efficiency. With reference to Table 2, it is clear that the efficiency of the system is not affected by sensor reduction. Furthermore, and from Table 4, the cost of one unit of the system with the reduced sensor approach is decreased by approximately 17% in comparison with full sensor utilization, which is considered a significant amount of reduction.

Moreover, the sensor reduction decreases the required number of analogue inputs of the real-time controller, which simplifies the overall control and decreases the computational power. In addition, sensor reduction or sensorless control is advantageous in case of sensor failure. In such a situation, it can be used as a backup strategy, which in turn increases the system reliability and enhance the system performance.

5.3 | Experimental set-up description

The studied system is composed of a PV emulator, boost converter, and resistive load. The PV emulator is established using a DC source and a group of resistors [39]. First, the DC source is connected with one resistor in series to emulate the P–V characteristic at a specific power level. After a permitted interval, another resistor is connected in parallel to the first one to mimic a rapid increase in the power (radiation). Finally, the attached resistor is disconnected to simulate a sudden decrease in the output power of the emulator. This is considered an effective and low-cost PV emulation system, which does not affect or alter the performance of the MPPT implementation. The output of the PV emulator is linked with the boost converter, which feeds

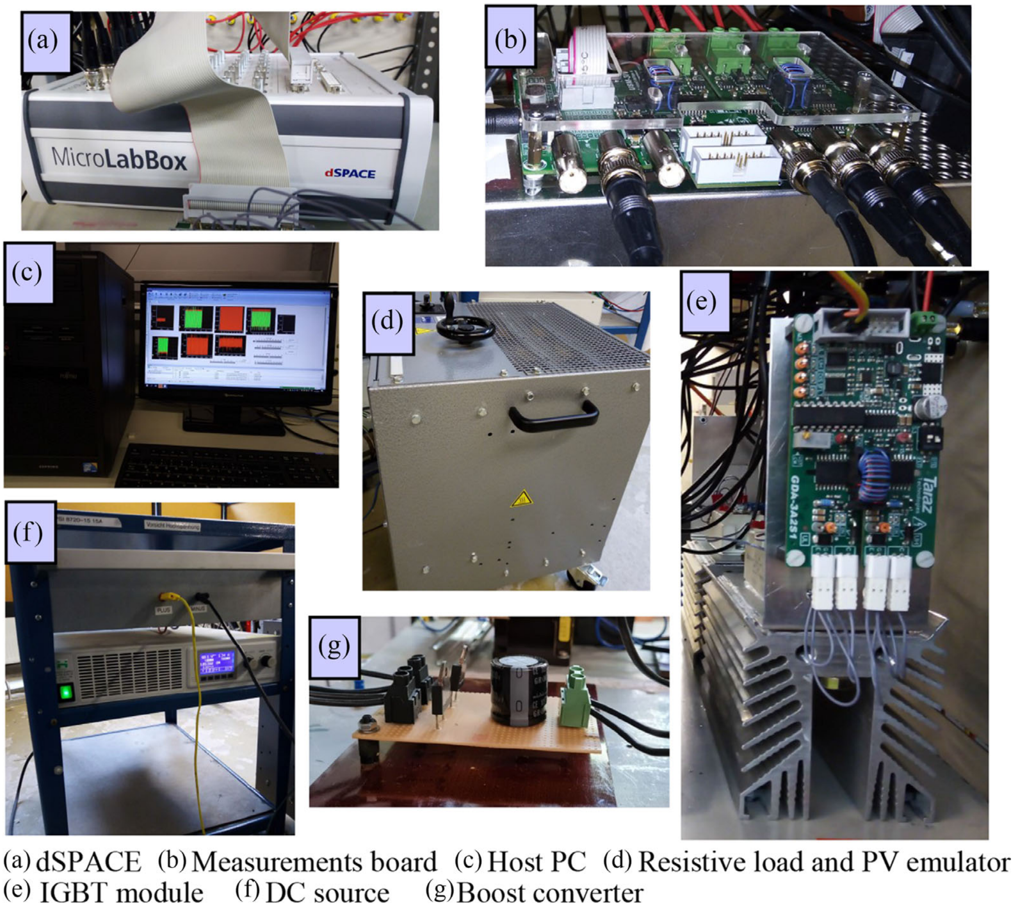

FIGURE 10 Hardware implementation of the PV emulation system with MPPT objective

TABLE 5 PV system parameters

Parameter	Value
Inductor (L)	8.5 mH
Output capacitor (c)	240 µF
Power switch	Single switch (IGBT-Module FF50R12RT4)
Diode (D)	Fast recovery diode BYW77PI200
Load (R)	30 Ω
PV emulator resistors	15 Ω/16.5 Ω
Sampling time (T_s)	100 µs

the resistive load. An isolated voltage and current sensing module (USM-3IV) is used to measure the PV voltage (v_{pv}), current (i_{pv}), and output capacitor voltage (v_c). These measurements are fed to dSPACE DS1202 MicroLabBox, which is employed as a real-time controller. The control algorithm is executed using MATLAB software, and hence the obtained switching state is applied to the switch. A smart gate drive (GDA-2A2S1) is utilized as an interface between the dSPACE and the power switch. Figure 10 shows the experimental configuration of the set-up, while the details of the whole PV system are summed up in Table 5.

5.4 | Experimental results and discussion

5.4.1 | MPPT performance at step-up changes of the PV power

Figure 11 shows the behaviour of the current-oriented FS-MPC algorithm under the step-up change condition of the PV power. The results show (from top to bottom) the PV power (p_{pv}) extracted from the PV emulator, the PV voltage (v_{pv}), the PV current (i_{pv}), the capacitor voltage (v_c), and the instantaneous efficiency (η_{pv}), respectively. The current-oriented MPPT algorithm successfully tracks the next power level when an abrupt power change happens. The steady-state ripple of the PV power is less than 2 W, which corresponds to 4% when compared with the PV power reference. The PV voltage exhibits a moderate overshoot, which is also addressed in [7, 13 24]. Correspondingly, the instantaneous efficiency drops during this interval. However, the instantaneous value of the efficiency at steady state is more than 95% (similar to the simulation case). For the voltage-oriented FS-MPC technique, shown in Figure 12, the same results are given, where the tracking speed of the PV power is faster than the current-oriented method. The steady-state ripple behaviour of the PV power is similar to the current-based one. Furthermore, the overshoot of the PV voltage waveform is medium like the case of the

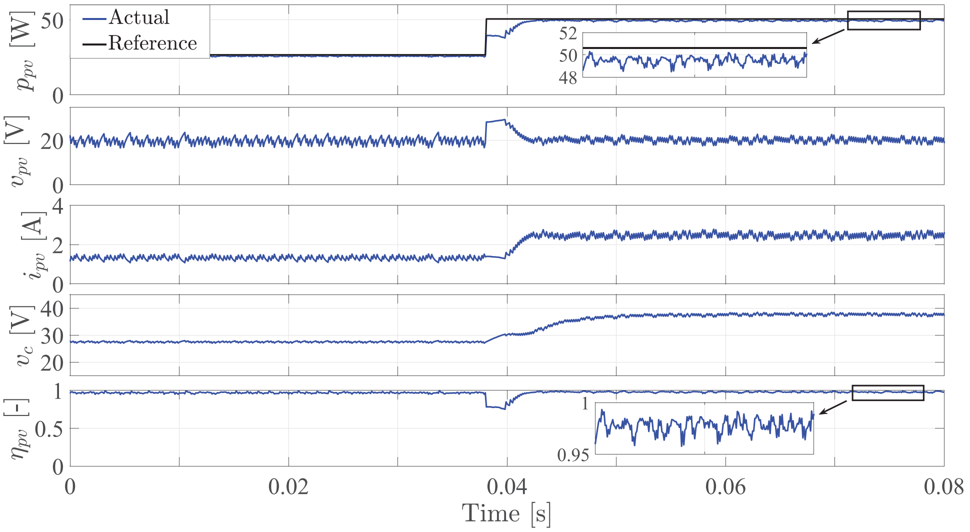

FIGURE 11 Experimental behaviour of the current-oriented FS-MPC MPPT under step-up change in the power

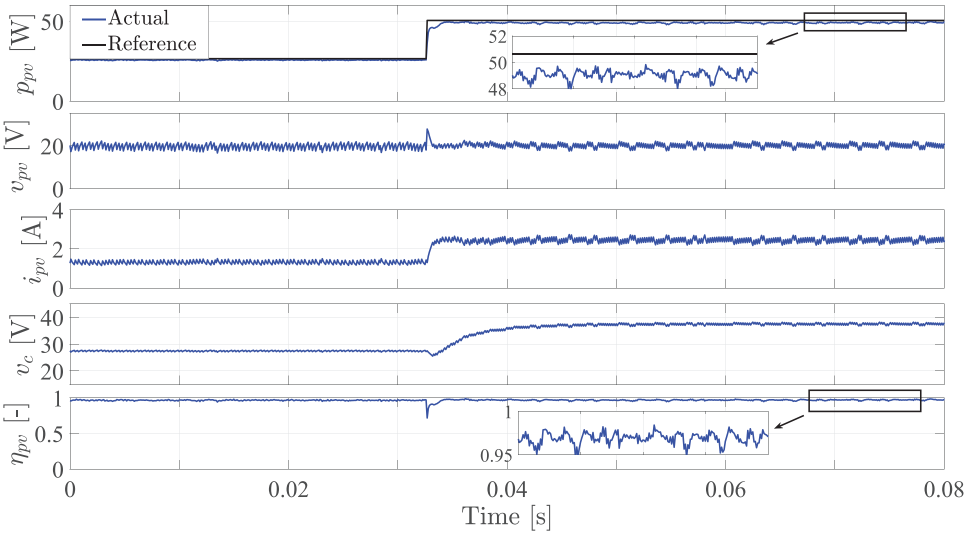

FIGURE 12 Experimental behaviour of the voltage-oriented FS-MPC MPPT under step-up change in the power

current-oriented method. Moreover, the value of instantaneous efficiency at steady state is a little bit lower when compared to the current technique.

Figure 13 also shows the same results but with the first reduced sensor count approach based on the losses model of the system. The PV power, voltage, current, and instantaneous efficiency show very similar behaviour to the voltage-based method. However, the estimated capacitor voltage has a faster transient response in comparison with the actual one. Even more, the estimation has lower ripple content compared to the measured value. For the EKF technique shown in Figure 14, the tracking speed of the PV power is fast. Furthermore, the ripple content is also limited to less than 2 W. The estimation of the PV current is very adequate. However, very small steady-state errors can be observed between the measured and estimated PV current. The average value of this error is 2.27%. This, in turn, causes a small deviation in the PV voltage waveform when the system transits from the lower to the upper power level. Nevertheless, this deviation does not affect the maximum power production. The drops of the instantaneous PV efficiencies are very similar for the voltage-oriented, losses model, and EKF technique when the step change happens.

5.4.2 | MPPT performance at step-down changes of the PV power

Figure 15 shows (from top to bottom) the PV power, the PV voltage, the PV current, the capacitor voltage, and the instantaneous efficiency at step-down changes of the PV power, respectively. For the current-based technique, one can observe that the PV power exhibits a relatively high undershoot, which is in conjunction with a very high undershoot in the PV voltage waveform. These drops are also reported in [23]. As the

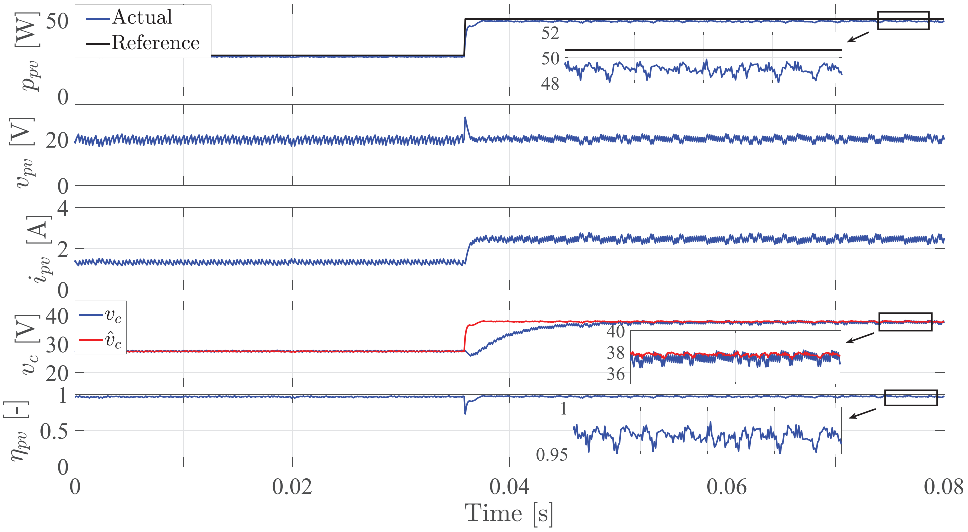

FIGURE 13 Experimental behaviour of the reduced sensor count FS-MPC-based losses model under step-up change in the power

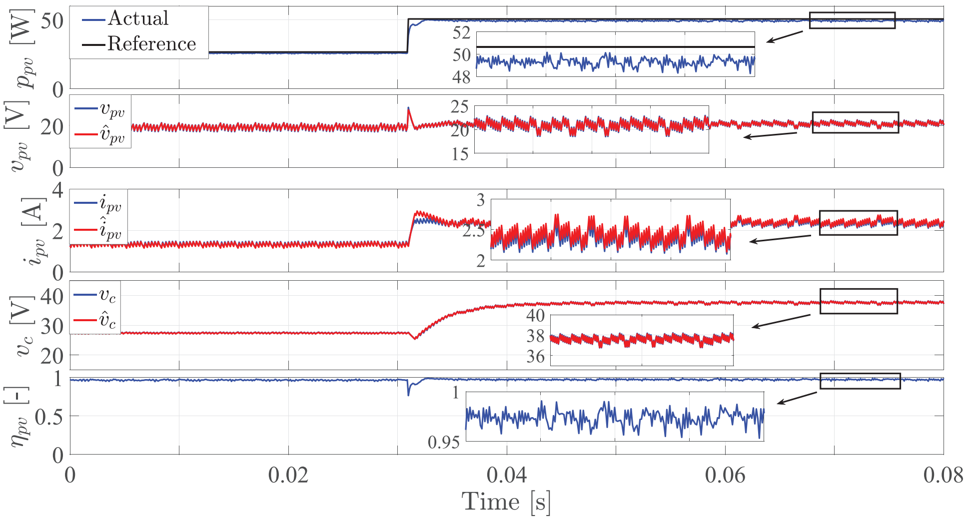

FIGURE 14 Experimental behaviour of the reduced sensor count FS-MPC-based EKF under step-up change in the power

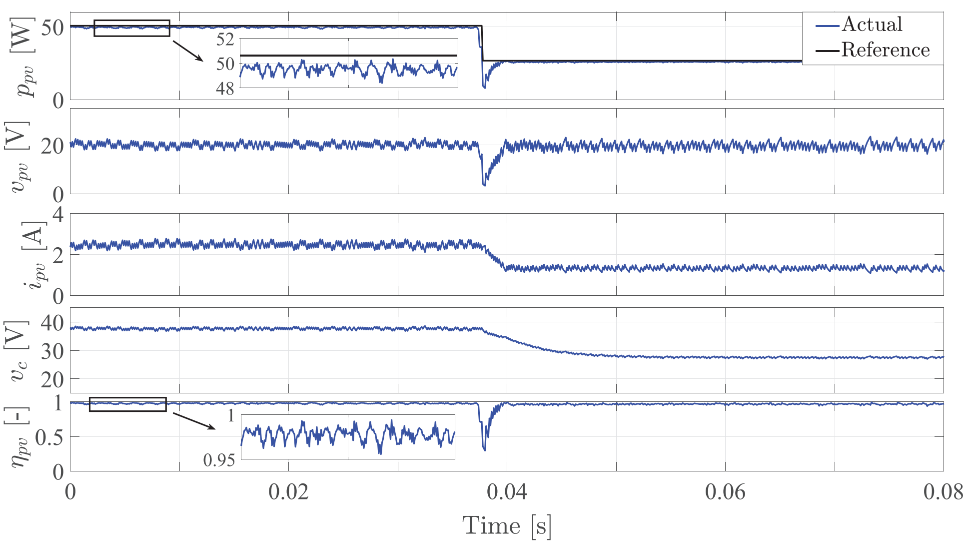

FIGURE 15 Experimental performance of the current-oriented FS-MPC MPPT under step-down change in the power

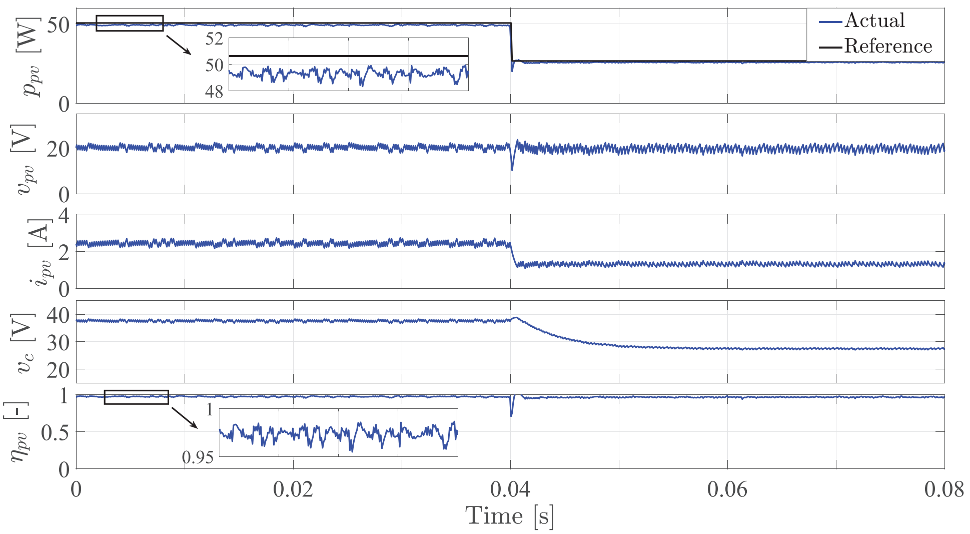

FIGURE 16 Experimental performance of the voltage-oriented FS-MPC MPPT under step-down change in the power

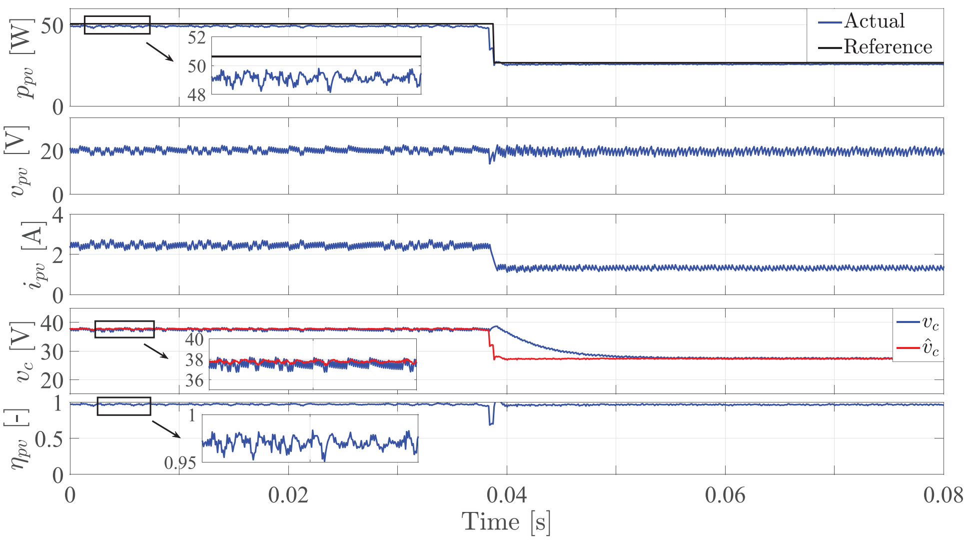

FIGURE 17 Experimental performance of the reduced sensor count FS-MPC-based losses model under step-down change in the power

controller is based on the current, therefore, at a sudden decrease in the power, the reference current is expected to decrease abruptly to track the maximum power. However, the inductor at the input side of the boost converter does not allow this fast change in the current, which in turn imposes a negative voltage. Thus, the PV voltage drops to a low value causing the same for the PV power. With the voltage-oriented method (Figure 16), the PV power shows a small undershoot. Furthermore, the PV voltage undershoot becomes smaller in comparison with the current-based algorithm. For the reduced sensor count techniques (losses model and EKF), which are presented in Figures 17 and 18, the PV power has a negligible undershoot corresponding to a low undershoot in the PV voltage waveform.

Briefly, the PV power ripple is about 2 W, which corresponds to 4% when compared to the PV power reference. The instantaneous efficiency is more than 95% under all operating conditions. Furthermore, Table 6 summarizes the transient behaviour of all studied methods.

Further insight is given into the reduced sensor count methods. As mentioned previously, the capacitor voltage estimation using the losses model reduces the sensor count by one. However, an accurate losses model should be developed for this purpose. The efficiency mentioned in Equation (7) accounts for the losses. As suggested by the authors, the average value of the efficiency over the operating range of the converter is considered for losses compensation. The analytical solution, based on the derived expression in Equation (7) and further investigated in the curve shown in Figure 3, is 96.89%. However, using online observation (control desk program) at different operating conditions, the optimum value for the efficiency is found to be 96.80%. The difference between the experimental and analytical efficiencies of the boost converter is very small. This proves the accuracy of the developed losses model.

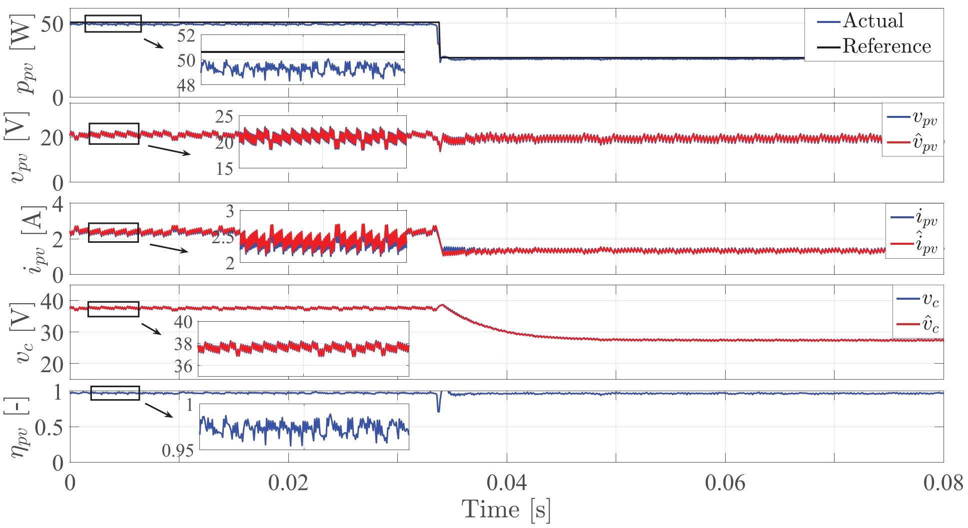

FIGURE 18 Experimental performance of the reduced sensor count FS-MPC-based EKF under step-down change in the power

TABLE 6 Transient performance summary of the MPPT techniques

Parameter	Current-oriented	Voltage-oriented	Estimation-based losses model	Estimation-based EKF
PV power overshoots (p_{pv})	No	No	No	No
PV power undershoots (p_{pv})	High	Small	Negligible	Negligible
PV voltage overshoots (v_{pv})	Moderate	Moderate	Moderate	Moderate
PV voltage undershoots (v_{pv})	Very high	Moderate	Low	Low
Instantaneous efficiency drops/at power drops (η_{pv})	Very high	Moderate	Moderate	Moderate

The EKF approach is used to eliminate the PV current sensor. However, during the estimation process, the PV voltage and the capacitor voltage are also estimated. These values can be used in the developed control strategy if the measurements contain noise (to make benefit from the filtering capability of the EKF). The estimation of the voltages is precise as shown in Figures 14 and 18. As discussed, the covariance matrices have a large impact on the performance of the EKF, and therefore on the estimation of the current. Thus, after the initial guess using the PSO method, the values are adjusted online for a better estimation using the control desk software. The final values of these matrices and initialization are given by

$x_0 = [0.01, 0.01, 0.01]^T$,
Q= diag (0.005,0.05,6),
R= diag (1,1), and
P_0= diag (1,1,1).

Furthermore, the sensor reduction-based losses model – as it considers output capacitor voltage elimination – affects only the prediction stage of the FS-MPC method. However, with the EKF, where the current sensor is eliminated, the reference calculation stage in addition to the prediction stage of the FS-MPC procedure are influenced (see Figure 5). In conclusion, the errors in the current estimation by the EKF will affect the reference generation leading to errors in the maximum power extraction. On the other side, the losses-based method has less impact as the voltage estimation procedure has no relation to the reference generation stage.

Another issue that should be considered when comparing the current-oriented technique and the voltage-oriented one is the tracking speed. With reference to the PV characteristics in Figure 1, it is obvious that with radiation change, the PV voltages are concentrated in a narrow range. However, the current variation range is wide. Thus, for the voltage-oriented method, the effort to track the maximum power in view of radiation change is small, as the MPP voltage is in the neighbourhood. In case of current, the tracking speed is expected to be slower than that of the voltage-based method, where the current is approximately proportional to the radiation. The tracking speed of all studied methods and the average efficiency are summed up in Table 7. The current-oriented method has a slightly higher average efficiency in comparison with other techniques, which is in very good agreement with the simulation results (see Table 2). The average efficiency value of the reduced sensor count approaches and the voltage-oriented technique are very comparable together, which proves the effectiveness of the proposed sensor reduction strategies. Furthermore, the tracking speed of the current-oriented strategy is the slowest

TABLE 7 Tracking speed and average efficiency of the MPPT techniques

Method	Tracking speed	$\eta_{pv,avg}$ (%)
Current-oriented	28 T_s	97.07
Voltage-oriented	4 T_s	96.93
Estimation-based losses model	4 T_s	96.70
Estimation-based EKF	4 T_s	96.85

TABLE 8 Execution time and average switching frequency for the MPPT algorithms

Method	Execution time (μs)	Avg. f_s (kHz)
Current-oriented	5.25	3.48
Voltage-oriented	5.26	3.69
Estimation-based losses model	5.82	3.66
Estimation-based EKF	6.18	3.82

when compared to the voltage-based methods. In the same context, the voltage-oriented algorithm, the reduced sensor count technique-based losses model, and the EKF approach have the same tracking speed, which means that the sensor reduction does not affect the MPPT transient behaviour.

Furthermore, the execution time and average switching frequency (f_s) for all studied methods are given in Table 8. The EKF approach has a relatively high execution time in comparison with other methods. This time is consumed in the prediction and correction stage of the EKF implementation. Nevertheless, it can be achieved within a very short time compared to the control cycle (sampling time). The current- and voltage-oriented methods have approximately the same execution time. The reduced sensor count-based losses model requires a little bit higher execution time when compared with the current and voltage methods. The current-based algorithm has the lowest average switching frequency, while other techniques have a comparable switching frequency. It is worth mentioning that at such operating switching frequency, the switching losses are very small to account for. Therefore, they can be neglected without affecting the quality of the estimated parameters.

5.5 | Robustness assessment

MPPT-based FS-MPC depends on the parameters of the utilized converter. Thus, the effect of these parameters on the control performance will be investigated. First, the effect of load changes on the behaviour of the MPPT is illustrated in Figure 19. Specifically, step-change variations are studied for the reduced sensor control strategies. A parallel branch is connected with the original load to emulate a step decrease in the load by approximately 25%. For the reduced current sensor technique with EKF, the power drops when the step change is applied to the load. The amount of reduction is about 0.6 W (avg.), which corresponds to a 2.74% decrease in the PV power. Furthermore, the ripple content of the PV power increases due to the errors in the current estimation, which result in operation near the MPP. However, with the reduced capacitor voltage sensor algorithm, the effect of the step change in the load is almost negligible on the power. Furthermore, the impact of boost inductance variations is conducted. The inductance variation has no effect on the reduced capacitor sensor technique, as the cost function design is independent of the inductance. However, the EKF approach depends moderately on the inductance variation. Figure 20 shows the influence of the inductance change on the power, where the produced power from the PV source decreases as the inductance value differs from the nominal value. Moreover, it is observable that the dependency on the inductance is unsymmetrical, where it is more notable with low inductance values. One can conclude that the reduced sensor technique based on the losses model is more robust than the EKF against parameters variation. It is worth mentioning that the effect of the output capacitance variation on the control performance is minor for both techniques.

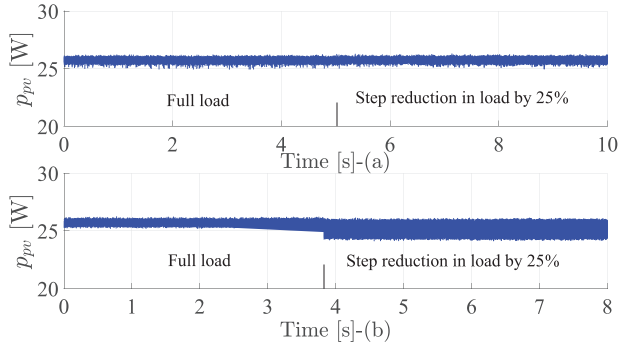

FIGURE 19 Effect of step change reduction in load on the reduced sensor count algorithms: (a) Reduced sensor-based losses model technique; (b) Reduced sensor based-EKF

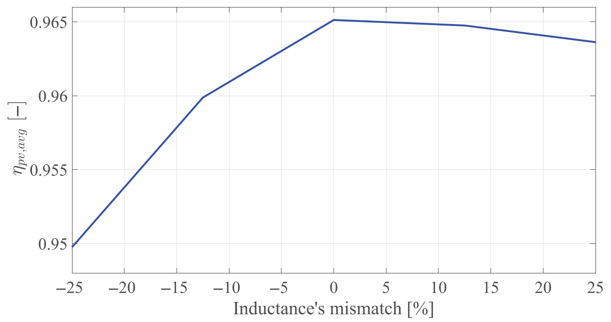

FIGURE 20 Effect of the inductance's mismatch on the average efficiency for the EKF method

5.6 | Comparative evaluation

Table 9 briefly compares all studied MPPT techniques. The number of utilized sensors, control parameter, the computational burden, the tracking speed, and the dependency on the utilized converters are considered to evaluate and compare

TABLE 9 Comparative evaluation of the MPPT techniques

Parameter	Current-oriented	Voltage-oriented	Estimation-based losses model	Estimation-based EKF
Number of sensors	3	3	2	2
Control parameter	Current	Voltage	Voltage	Voltage
Execution time	Low	Low	Moderate	High
Tracking speed	Fast	Very fast	Very fast	Very fast
Parameter's dependency	Low	Low	Low	Moderate

the algorithms. The current-oriented algorithm utilizes the current as a control parameter. The voltage is employed in the other methods (voltage-based, losses model, and EKF). The EKF approach has the highest computational burden among all studied methods. Furthermore, it is more dependent on the converter's parameters. Voltage-dependent methods have the fastest tracking speed. However, current-based methods are relatively slower.

6 | CONCLUSION

An overview of MPPT-based FS-MPC has been presented in this paper. Furthermore, two approaches have been utilized to reduce the required sensors for implementation. The first approach uses an accurate model of the PV system, where the losses of the converter are included to estimate the output capacitor voltage. The second approach makes benefit from the developed losses model and integrates it with the EKF observer to eliminate the PV current sensor. In addition, current- and voltage-oriented algorithms with full sensor utilization are studied for comparison and evaluation. Cost comparison has indicated that the most effective method to reduce the cost of the PV system is sensor elimination. In this matter, approximately a 17% reduction in the cost is achieved with a negligible effect on the system's efficiency. In terms of efficiency, all methods have a very similar efficiency under step change of power (radiation). Voltage-based techniques have the fastest tracking speed, whereas the current-based method gives the worst transient behaviour. Furthermore, the EKF technique is more dependent on the converter parameters. According to a dynamic test of radiation, the PV efficiency is reduced due to the drift problem. Nevertheless, the reduction is not significant due to the fast transient behaviour of the FS-MPC. When considering sensor reduction, it is not recommended to eliminate the PV current sensor as it may lead to false operation of MPPT when the system is subjected to parameter uncertainties. Sensor reduction is preferred as a backup control strategy to enhance system reliability.

ACKNOWLEDGEMENTS

The work of Jose Rodriguez was supported by Agencia Nacional de Investigación y Desarrollo (ANID) under Project FB0008, Project ACT192013, and Project 1210208.

CONFLICT OF INTEREST

The authors declare that there is no conflict of interest that could be perceived as prejudicing the impartiality of the research reported.

DATA AVAILABILITY STATEMENT

Data available on request from the authors.

ORCID

Mostafa Ahmed https://orcid.org/0000-0002-9036-059X
Mohamed Abdelrahem https://orcid.org/0000-0003-2923-2094

REFERENCES

1. Hemeida, A.M., et al.: Optimum design of hybrid wind/PV energy system for remote area. Ain Shams Eng. J. 11(1), 11–23 (2020)
2. Mostafa, A., et al.: An adaptive model-based MPPT technique with drift-avoidance for grid-connected PV systems. Energies 13(24), 6656 (2020)
3. Mostafa, A., et al.: DC-link sensorless control strategy for grid-connected PV systems. Electr. Eng. 103(5), 2345–2355 (2021)
4. Balakrishnan, P., et al.: Current status and future prospects of renewable energy: A case study. Energy Sources Part A 42(21), 2698–2703 (2020)
5. Haidar, I., et al.: Performance evaluation of maximum power point tracking approaches and photovoltaic systems. Energies 11(2), 365 (2018)
6. Mostafa, A., Abdelrahem, M., Kennel, R.: Highly efficient and robust grid connected photovoltaic system based model predictive control with kalman filtering capability. Sustainability 12(11), 4542 (2020)
7. Morcos, M., et al.: MPPT of photovoltaic systems using sensorless current-based model predictive control. IEEE Trans. Ind. Appl. 53(2), 1157–1167 (2016)
8. Trishan, E., Chapman, P.L.: Comparison of photovoltaic array maximum power point tracking techniques. IEEE Trans. Energy Convers. 22(2), 439–449 (2007)
9. Kashif, I., Salam, Z.: A review of maximum power point tracking techniques of PV system for uniform insolation and partial shading condition. Renewable Sustainable Energy Rev. 19, 475–488 (2013)
10. Podder, A.K., Roy, N.K., Pota, H.R.: MPPT methods for solar PV systems: A critical review based on tracking nature. IET Renewable Power Gener. 13(10), 1615–1632 (2019)
11. Sera, D., et al.: On the perturb-and-observe and incremental conductance MPPT methods for PV systems. IEEE J. Photovoltaics 3(3), 1070–1078 (2013)
12. Motahhir, S., El Hammoumi, A., El Ghzizal, A.: The most used MPPT algorithms: Review and the suitable low-cost embedded board for each algorithm. J. Cleaner Prod. 246, 118983 (2020)
13. Shadmand, M., Balog, R.S., Rub, H.A.: Maximum power point tracking using model predictive control of a flyback converter for photovoltaic applications. In: Power and Energy Conference at Illinois (PECI), pp. 1–5. IEEE (2014)
14. Sher, H.A., et al.: A new sensorless hybrid MPPT algorithm based on fractional short-circuit current measurement and P&O MPPT. IEEE Trans. Sustainable Energy 6(4), 1426–1434 (2015)
15. Abouadane, H., et al.: Multiple-power-sample based P&O MPPT for fast-changing irradiance conditions for a simple implementation. IEEE J. Photovoltaics 10(5), 1481–1488 (2020)
16. Padmanaban, S.K., et al.: A novel modified sine-cosine optimized MPPT algorithm for grid integrated PV system under real operating conditions. IEEE Access 7, 10467–10477 (2019)
17. Salam, Z., Ahmed, J., Merugu, B.S.: The application of soft computing methods for MPPT of PV system: A technological and status review. Appl. Energy 107, 135–148 (2013)
18. Kermadi, M., et al.: Recent developments of MPPT techniques for PV systems under partial shading conditions: A critical review and performance evaluation. IET Renewable Power Gener. 14(17), 3401–3417 (2020)

19. Manoharan, P.K., et al.: Improved perturb and observation maximum power point tracking technique for solar photovoltaic power generation systems. IEEE Syst. J. 15(2), 3024–3035 (2020)
20. Karamanakos, P., et al.: Model predictive control of power electronic systems: Methods, results, and challenges. IEEE Open J. Ind. Appl. 1, 95–114 (2020)
21. Abdelrahem, M., et al.: Robust predictive control for direct-driven surface-mounted permanent-magnet synchronous generators without mechanical sensors. IEEE Trans. Energy Convers. 33(1), 179–189 (2017)
22. Kakosimos, P.E., Kladas, A.G.: Implementation of photovoltaic array MPPT through fixed step predictive control technique. Renewable Energy 36(9), 2508–2514 (2011)
23. Kakosimos, P.E., Kladas, A.G., Manias, S.N.: Fast photovoltaic-system voltage-or current-oriented MPPT employing a predictive digital current-controlled converter. IEEE Trans. Ind. Electron. 60(12), 5673–5685 (2012)
24. Mosa, M., et al.: Efficient maximum power point tracking using model predictive control for photovoltaic systems under dynamic weather condition. IET Renewable Power Gener. 11(11), 1401–1409 (2017)
25. Abushaiba, A.A., Eshtaiwi, S.M.M., Ahmadi, R.: A new model predictive based maximum power point tracking method for photovoltaic applications. In: IEEE International Conference on Electro Information Technology (EIT), pp. 571–575. IEEE (2016)
26. Sajadian, S., Ahmadi, R.: Model predictive-based maximum power point tracking for grid-tied photovoltaic applications using a Z-source inverter. IEEE Trans. Power Electron. 31(11), 7611–7620 (2016)
27. Lashab, A., Sera, D., Guerrero, J.M.: A dual-discrete model predictive control-based MPPT for PV systems. IEEE Trans. Power Electron. 34(10), 9686–9697 (2019)
28. Hussain, A., et al.: Improved restricted control set model predictive control (iRCS-MPC) based maximum power point tracking of photovoltaic module. IEEE Access 7, 149422–149432 (2019)
29. Ahmed, M., et al.: A robust maximum power point tracking based model predictive control and extended Kalman filter for PV systems. In: International Symposium on Power Electronics, Electrical Drives, Automation and Motion (SPEEDAM), pp. 514–519. IEEE (2020)
30. Abdel-Rahim, O., Wang, H.: A new high gain DC-DC converter with model-predictive-control based MPPT technique for photovoltaic systems. CPSS Trans. Power Electron. Appl. 5(2), 191–200 (2020)
31. Lashab, A., et al.: Discrete model-predictive-control-based maximum power point tracking for PV systems: Overview and evaluation. IEEE Trans. Power Electron. 33(8), 7273–7287 (2017)
32. Ahmed, J., Salam, Z.: A modified P&O maximum power point tracking method with reduced steady-state oscillation and improved tracking efficiency. IEEE Trans. Sustainable Energy 7(4), 1506–1515 (2016)
33. Ahmed, J., Salam, Z.: An improved perturb and observe (P&O) maximum power point tracking (MPPT) algorithm for higher efficiency. Appl. Energy 150, 97–108 (2015)
34. Ishaque, K., Salam, Z., Lauss, G.: The performance of perturb and observe and incremental conductance maximum power point tracking method under dynamic weather conditions. Appl. Energy 119, 228–236 (2014)
35. Li, X., et al.: A comparative study on photovoltaic MPPT algorithms under EN50530 dynamic test procedure. IEEE Trans. Power Electron. 36(4), 4153–4168 (2020)
36. Allwyn, R.G., et al.: Economic analysis of replacing HPS lamp with LED lamp and cost estimation to set up PV/battery system for street lighting in Oman. Energies 14(22), 7697 (2021)
37. Xiao, W., et al.: Review of grid-tied converter topologies used in photovoltaic systems. IET Renewable Power Gener. 10(10), 1543–1551 (2016)
38. Zeb, K., et al.: A comprehensive review on inverter topologies and control strategies for grid connected photovoltaic system. Renewable Sustainable Energy Rev. 94, 1120–1141 (2018)
39. Zakzouk, N.E., et al.: PV single-phase grid-connected converter: DC-link voltage sensorless prospective. IEEE J. Emerging Sel. Top. Power Electron. 5(1), 526–546 (2016)

How to cite this article: Ahmed, M., Harbi, I., Hackl, C.M., Kennel, R., Rodriguez, J., Abdelrahem, M.: Maximum power point tracking-based model predictive control with reduced sensor count for PV applications. IET Renew. Power Gener. 19, e12535 (2025). https://doi.org/10.1049/rpg2.12535